Pergamon

Planet. Space Sci., Vol. 46, No. 5, pp. 547–553, 1998

0032–0633/98 $19.00+0.00

PII: S0032–0633(97)00122–0

First images of a comet with adaptive optics

O. Marco,[1,2] **T. Encrenaz**[1] **and E. Gendron**[1]

[1]Observatoire de Paris-Meudon, F-92190, Meudon, France
[2]Université Pierre et Marie Curie, F-75252, Paris, France

Received 7 November 1996; revised 15 May 1997; accepted 21 May 1997

Abstract. Using the ADONIS adaptive optics system at ESO (La Silla, Chile), on 8 March 1996, we made the very first observation of a comet with adaptive optics. Comet C/1996 B2 (Hyakutake) has been imaged in the near-infrared (J, H, K bands at 1.2, 1.6 & 2.2 μm respectively). The achieved spatial resolution of $\approx 0.2''$, has allowed us to isolate two distinct dust-colour regions in the immediate neighbourhood of the cometary nucleus. On a [J–H] colour index map, a bluer region has been detected in the sunward-facing hemisphere, while a redder one is located symmetrically in the anti-solar direction. The major dust component in the coma remains silicates. These new observations should help to constrain the current models for dust components in comets. They clearly demonstrate the feasibility of observing comets with adaptive optics systems. Future observations of comet Hale–Bopp should greatly benefit from this new technique.

Introduction

Atmospheric turbulence, responsible for "seeing" effects, leads to severe limitations on the spatial resolution of ground-based telescopes. Basically, the angular resolution achieved on large telescopes is of the order of 1″, and even on an excellent site, it is limited to 0.35″ in the very best case.

As they correct for atmospheric effects on ground based-telescopes, adaptive optics systems allow us to approach the diffraction limit and to image comets at high angular resolution. We used the ADONIS ESO adaptive optics system (Beuzit *et al.*, 1994) on the 3.6 m telescope (La Silla, Chile) to observe comet C/1996 B2 (Hyakutake) in the near infrared, on 8 March 1996.

The ADONIS system performs real-time correction and compensation of wavefront distortions due to the atmospheric turbulence, as well as for the telescope optical aberrations, such as defocus and coma, etc. The basic concept of adaptive optics is to measure the phase perturbations with a wavefront analysis sensor using the visible part of the object light (or a bright closed reference star), and to introduce phase corrections, opposite to the distortions, in the optical path with a deformable mirror. ADONIS is equipped with an optimised modal control and an artificial intelligence system, to ensure optimal performance. A variety of input parameters, such as magnitude and spectral type of the objects used for wavefront sensing, the atmospheric turbulence profile, and overall meteorological conditions, are handled by the artificial intelligence system with the aim to achieve the best possible image quality. A detailed instrumental description can be found in Saint-Pé *et al.* (1993).

Observations and reductions

The wavefront analysis of the adaptive optics system was performed directly on the cometary nucleus, as it was bright enough: its visual magnitude was 14.7 (ephemeris measurement), in addition to the bright central part of the coma (extended source of visual magnitude 5.8). The telescope tracking was fully compensated by the adaptive optics system, allowing long exposure times without any shifting due to the comet proper motion. As a comparison, when the comet Hyakutake was observed with the ESO NTT on 19–20 March 1996 (O. Hainaut and R. West), its extremely rapid motion was about 0.75″/s. To observe at the best seeing resolution ($\approx 0.5''$ at NTT at this period) with an individual frame exposure time of 3 s, the observers needed a very highly accurate ephemeris. With an adaptive optics system, this is not necessary, since the tilt mirror corrects in real time the object shifts. We measured the achieved spatial resolution by observing stars with the same adaptive optics correction. As adaptive optics systems only partially correct for wavefront distortions, the uncompensated light forms a halo around the (alsmost) diffraction limited core. The performance of an adaptive optics system is generally described by the Strehl ratio, which is the ratio of the maximum intensity

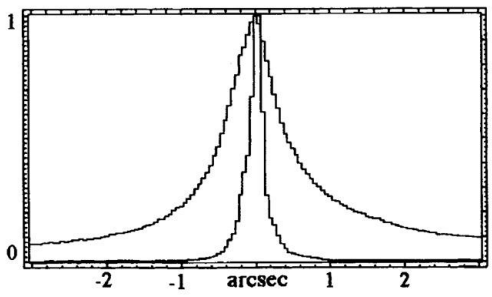

Fig. 1. Cut of the comet and the PSF in the K band

obtained in a point source image to the maximum intensity in the diffraction limited image (Airy pattern). A perfect correction would correspond to a Strehl ratio of 1 ; typical values for faint sources are currently 5–25%, and increase with λ. To estimate the image quality, one can also measure the full width at half maximum (FWHM) of a point spread function (PSF) star, but it is not as precise as the Strehl ratio. For a same FWHM of a PSF star, the Strehl ratio can differ by a few percent : this is not incompatible, as the FWHM is indicative of the spreading of the image, which is limited by the diffraction effect, whereas the Strehl ratio is sensitive to the relative energy distribution between the peak and the halo. For instance, during the observations related here, we obtained two PSF in the H band, separated by 2.5 h, with a same FWHM but a Strehl ratio differing by 1% : this indicates that the adaptive optics correction was more efficient in the later case. We summarize in Table 1 the technical description of the observations, and Fig. 1 presents a cut through the comet and its PSF in the K band.

To optimise the observations procedure, we used standard sequences for the filters : for each band, we made images and sky for these images (sky 1, band 1, band 2, sky 2), then a reference star for each band (a PSF and a photometric standard), then a new sequence, and so on. In order to calibrate the adaptive optics correction properly, we chose a $m_v = 9.3$ PSF reference star separated from the comet by only 3.5° to guarantee a similar adaptive optics correction. We have obtained several sets of images (J and H, H and K) but at the date we made the observations, the rotation period of the nucleus was not known. Due to the long exposure time, some data sets were separated by a few minutes, others by half an hour. Thus, after reducing the data, we kept only the data sets of two bands for which the rotation of the nucleus between these images was less significant than our spatial resolution. We reduced the data in a standard way : sky subtraction, flat-fielding and dead-pixels removal. We did not apply any non-linear process such as deconvolution to keep the photometry unchanged. We used the PSF reference star to measure the effective angular resolution : as the angular resolution is different between the J, H and K bands, we had to smooth the images to the same resolution before comparing them (the H image resolution to the J one, and the K one to the H one). Then, the photometric standards allowed us to compute the colour maps. As the comet was at a distance of 0.59 AU from the Earth, we resolved that the smallest details correspond roughly to 90 km ($\sim 0.2''$) at that distance (see Tables 1 and 2).

Results and discussion

On the basis of Campins and Hanner (1982) studies, we know that no strong gaseous signature is expected in the near infrared wavelengths (1–2.5 μm). Maillard *et al.* (1987) analysed the spectrum of P/Halley between 0.9 and 2.5 μm. In the 1–2.5 μm region, the only detected emissions were CN at 1.10 and 1.46 μm, C_2 at 1.45 μm, and an unidentified feature at 2.44 μm. Nevertheless, they were not in the standard filters bandwidth (the 1.10 μm CN emission is just in the down limit of the J band filter). Thus, this region is efficient for observing the solar light scattered by the particles.

Photometric measurements in the standard J, H and K bands are useful for deriving constraints upon the nature and distribution of cometary dust. The colour properties of the light scattered by the cometary dust has been analysed in detail by Campins and Hanner (1982), as a function of the scattering angle. They compared observations with models for absorbing and silicate grains, but their lack of spatial resolution made it difficult to conclude on the nature of dust. In a photometric aperture of several seconds, the measured colour index results from a mixture of particle size, composition and shape, furthermore, there is no obvious way to discriminate between these effects. For instance, from infrared photometry of comet P/Crommelin, Encrenaz *et al.* (1984) noticed an important colour index variation when changing the photometric aperture size. A possible explanation was that with a smaller diaphragm, the contribution of a dirty ice grains component would be more sensitive. This interpretation can be extended to all minority particles, which come to be detectable at high angular resolution. Thus, our images provide spatial information about the distribution of the dust surrounding the nucleus, at a small distance scale.

At an heliocentric distance >1 AU, there is no contamination at these wavelengths from thermal emission (A'Hearn *et al.*, 1981 ; Campins *et al.*, 1982 ; Veeder and Hanner, 1981) : the crossover from scattered to thermal emission occurs at ~ 3 μm at 1 AU. For our observations, the comet was at 1.39 AU from the Sun. We expect a blackbody temperature of about 250 K (Ney, 1974a ; Ney, 1974b), so we consider that all the brightness is caused by sunlight reflected in the dust grains. Water is the most abundant molecule in a comet nucleus (about 80% in Halley, Sagdeev *et al.*, 1986) and the comet was close enough to the Sun for water ice on its surface to evaporate freely. The dust is mostly released by this process, as the water vapour accelerates the dust grains outwards, away from the surface of the nucleus. Observations of the comet spectrum show strong emission lines or bands of CN, OH, HCN, CO, CS and C_2, and weaker emission by C_3 and NH_2. The measured gas production rates (IAU Circular, 1996, 6335) indicate on 2 March 1996 (a few days before our observations), that this comet is about as active as P/Halley at the same heliocentric distance ($r_h = 1.5$ AU), showing that it is a major comet. The nucleus diameter of comet Hyakutake has been determinated by NASA/JPL radar observations (S. Ostro, 1996), and is approximately 3 km, which is smaller than P/Halley. This high activity rate may mean that Hyakutake is younger than P/Halley, or that the active area on comet Hyakutake nucleus is significantly greater than P/Halley's. Infrared photometry

Table 1. Technical description of the observations

	Band	T_{obs} (UT)	T_{int}	S/B	FWHM comet	FWHM PSF	$1.22\,\lambda/D$	Strehl ratio
[J–H]	J	7:06 h	45 s	24	0.95″	0.25″	0.09″	5%
	H	7:00 h	30 s	23	0.90″	0.18″	0.12″	13%
[H–K]	H	9:25 h	30 s	27	0.85″	0.18″	0.12″	14%
	K	9:31 h	30 s	44	0.80″	0.15″	0.15″	23%
Jets	J	9:00 h	60 s	37	0.93″	0.25″	0.09″	5%

Table 2. Parameters relevant to comet Hyakutake observations

Name	C/1996 B2
Time of observations (UT)	March, 8.3, 1996
α_{2000}	14 h 54 m 21.7 s
δ_{2000}	−20°8′34″
m_v coma	5.8 (ephemeris estimation)
m_v nucleus	14.7 (ephemeris estimation)
Δ	0.59 AU
r_h	1.39 AU
Phase angle υ	120°
Pixel size	0.05″
Field of view	12.8″ × 12.8″
Spatial resolution in the coma	≈0.2″ (90 km)

of comet Hyakutake has been made on 21 March 1996, with the 0.763 m telescope at O'Brien Observatory with a 27″ circular aperture bolometer (Mason *et al.*, 1996); 10 and 20 μm silicate emission features were detected.

The ejection of dust particles from the surface of the cometary nucleus may also occur in strong jets. In comet Hyakutake, such jets have been observed (Jorda *et al.*, 1996). Figure 2 shows the ratio of two J band images separated by 2 h. We see a well indicated clockwise rotation of about 120°–180°, from which we can derive a rotation period ranging from 4–6 h. This is in reasonable agreement with the 6 h determination obtained in the visible range, based on imaging results combined with light-curve results, by Lecacheux *et al.* (1996). There is a strong dust jet and a very faint one, which is in good agreement with the assumption that only one very active region controls the photometric variations of the light-curve (IAU Circular, 1996, 6372). As a jet requires an active region to be located not too far from the nucleus equator, we deduce that the equator plane is roughly perpendicular to the line of sight. This is in agreement with Jorda *et al.*'s conclusions (IAU Circular, 1996, 6344), for the same period, that the nucleus shows its southern hemisphere to earth-based observers, and that the subsolar point lies near the comet equatorial plane.

From the three distinct photometric bands, we can compute two colour-index maps, [J–H] and [H–K]. As a comparison, we compute a colour index for the coma from an other photometric measurement by Lisse and A'Hearn (1996), made on 7 February 1996, at a distance from the Sun $r_h = 2$ AU, and $\Theta = 88°$: [J–H] = 0.4 and [H–K] = 0.1. As no image was recorded, we get no information on the spatial distribution of the dust, and what is derived is only the mean composition of the dust on a several thousand kilometre scale. In contrast, the excellent spatial resolution achieved in our measurements allows us to analyse in detail the dust colour and its spatial distribution. We present in Figs 3 and 4 colour images of the coma around the comet nucleus. To improve the legibility (filter the noise), the images have been smoothed with a 5-pixel (100 km) median filter.

Figure 3 is based on the colour index [J–H], derived from our images on 8 March, 7:00 h UT. Regarding the spatial distribution of the colour-index, we find three distinct dust-colour regions: for each region, we compute the mean colour-index value, and the error bar corresponds to the dispersion around this value. So, each region presented here corresponds to a unique colour-index. The first region, with a colour-index of 0.30 ± 0.02, is significantly bluer than the overall dust-colour index deduced from the 7 February data. This region (blue region in Fig. 3) is well localised, pointing directly toward and rather symmetrically around the projected solar vector. We also detect a redder colour index region with a well defined localisation (red colour in Fig. 3), located rather symmetrically from region 1, in the anti-solar direction. The colour index of this second region is 0.50 ± 0.03. The colour index of the remaining dust, with a 0.37 ± 0.05 value, is in good agreement with the 7 February data.

Figure 4 is based on the colour index [H–K], derived from our images on 8 March, 9:27 h UT, that is two hours and a half later than the [J–H] colour map. We isolate two regions. The first region (blue in Fig. 4) has a colour-index of 0.29 ± 0.05, is located in the sunward hemisphere, spatially limited, and centred on the nucleus with a night-/day effect. The second region (yellow in Fig. 4), with a colour index of 0.16 ± 0.05, is redder than the same colour index deduced from the 7 February data.

Infrared photometry measures primarily the radiation from the small dust particles in the coma. The colour of the light scattered by the grains depends on the particle size, shape, and composition, as well as the phase angle. Based on a model predicting the colour index for several kinds of dust components, we make an attempt to derive the nature of dust in comet Hyakutake. However, it has to be mentioned that our conclusion is not unambiguous, because different kinds of grains could eventually lead to the same colour index, and so the solution is not unique. We show in Fig. 5 the two colour indexes [J–H] and [H–K] plotted as functions of the scattering angle υ, computed from Mie scattering theory (Veeder and Hanner, 1981; Campins and Hanner, 1982). The authors select micron-

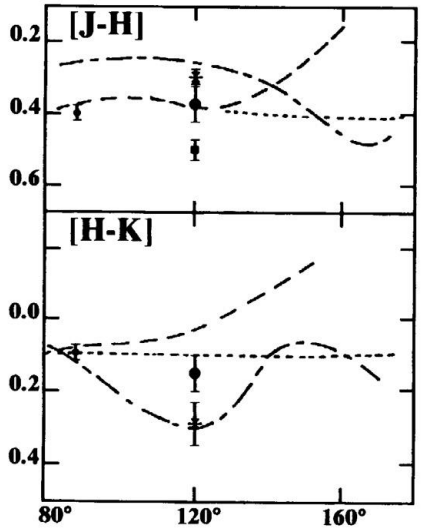

Fig. 5. [J–H] and [H–K] diagrams as a function of the scattering angle, from Veeder and Hanner (1981) and Campins and Hanner (1982). The dashed curves refer to silicate grains. The dotted lines represent the colour from the scattering by irregularly shaped silicate grains. The dash–dot curves correspond to the scattering by 20 μm grains of slightly dirty ice. The measurements at $\upsilon = 88°$ are from IAUC No. 6336. The others ($\upsilon = 120°$) are from our data; in that case, each point corresponds to an isolated dust-coulour region

sized silicates grains and 20 μm grains of slightly dirty ice, and they compute their expected colour index as functions of the scattering angle. We report in that figure our measurements, and other photometric measurements made on 7 February (IAU Circular, 1996, 6336). From our data, we plot only three points in the case of the [J–H] image, and two for the [H–K] image, corresponding to the three (respectively two) regions of different colour index shown in our images.

The colour indexes calculated from the 7 February data in [J–H] and [H–K] correspond to silicate dust, according to the model. This is in agreement with the detection of a silicate emission feature at 10 and 20 μm (IAU Circular, 1996, 6365). At that distance from the Sun, $r_h = 2$ AU, icy grains would not survive long enough to make a significant contribution to the cometary flux on scales larger than a few hundred kilometres (Hanner, 1981). So, in these conditions, we do not expect to detect them through their effect on the dust colour. The dust cannot be a mixture between silicates and more absorbing material, as it would become redder than it is. For the same reason, the size of the silicate grains is rather small, as otherwise it would be more reddish. Thus, this leads us to believe that the two measurements are in good agreement with a silicate composition of small grains. Even if there were a small amount of ice, or any other minority particle, it would not be detectable because of the lack of spatial resolution.

We derive three distinct colour-dust regions from the [J–H] index, plotted in Fig. 5. The 0.37 ± 0.05 value is consistent with a silicate dust composition, and is found to be the major dust component of the coma. It is in good agreement with the low-resolution previous observations (7 February data). The 0.30 ± 0.02 value is compatible with a dust composition of dirty ice grains. This is underlined by the well localised distribution of this dust in the image (blue region), pointing directly toward and rather symmetrically around the projected solar vector. The limited spatial distribution of that dust component can be due to the sublimation of the grains, and their size (about 20 μm, which is bigger than silicate grains), which explain their anisotropic distribution. We also detect a redder region of 0.50 ± 0.03, with a well defined location. A small amount of absorbing material in the silicate matrix would tend to make the colour redder than the colour computed for pure silicate spheres. Nevertheless, the observed spatial distribution is not compatible with that interpretation, as in that case we would expect a rather isotropic distribution. On the other side, the spatial distribution of that region can be explained by the presence of more massive grains. When the dust is ejected from the nucleus, it is accelerated by the gas outflow. The terminal velocity of a solid grain is primarily a function of the gas flux leaving the nuclear surface (Hanner, 1981). The acceleration effect is strongest on the small grains, which are therefore first swept away, so the larger grains stay longer in the neighbourhood of the cometary nucleus. This can induce the colour differences between the inner and outer coma reported here. Under that picture, this region would be the result of a size effect.

We also plot in Fig. 5 the [H–K] colour-index, from which we derive a two component dust model. The first component has a colour-index of 0.29 ± 0.05. This region is located in the sunward hemisphere, spatially limited, and centred on the nucleus with a night/day effect. Based on the model, a possible interpretation for the composition of these grains is an icy component, whose location is in good agreement with the observations from the 7:00 h image. Once again, the limited spatial distribution of that dust component can be due to size effects, and to the sublimation of the grains, which is much faster for icy grains than for others. The remaining dust has a colour index of 0.16 ± 0.05, redder than the February [H–K] measurements. As we know from the earlier measurements, the silicate grains are rather small on a large scale. So, this redder colour index may be the result of a size effect, indicating that substantially bigger grains are surrounding the immediate neighbourhood of the nucleus. This interpretation is in agreement with the [J–H] image, where we seem to detect more massive grains near the nucleus.

We notice important changes in the broadband colours and in the spatial distribution of the dust between the [J–H] and [H–K] images, separated by 2.5 h, reflecting the appearance of different dust regimes in the coma. This can be caused either by a heterogeneous rotating cometary nucleus, or by short time-scale variable activity of the nucleus. In the earlier configuration, the putative icy grains may be ejected with a velocity larger than for the later. Therefore, with the same lifetime, the icy grains would go much farther from the nucleus before sublimating. Using the models developed by Hanner (1981), we assume a velocity of 260 m s^{-1} for the icy grains (20 μm sized) and we deduce from the size of the ice halo in the later picture, a lifetime of 1000 s, in good agreement with the models. Thus, we can compute an icy grain velocity of about 700 m s^{-1} for the earlier configuration. Never-

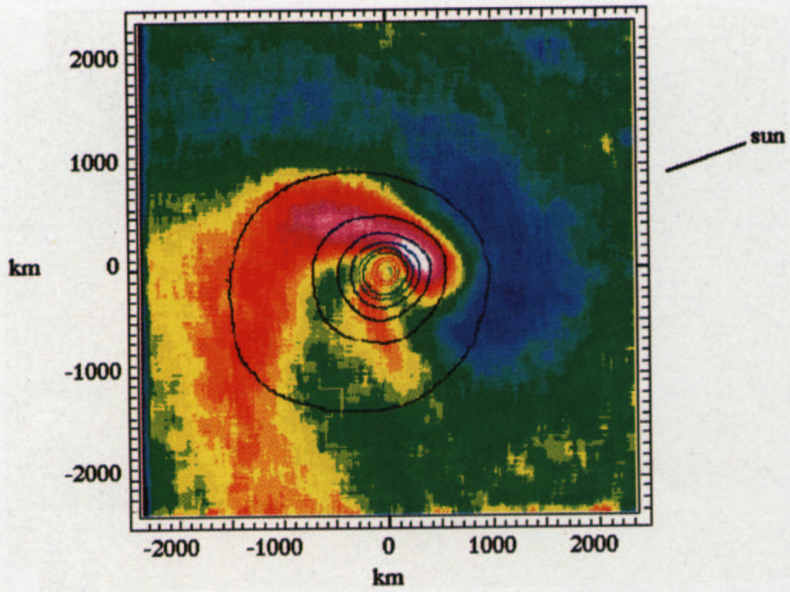

Fig. 2. The colour map presents the ratio of the 7:06 h UT image to the 9:00 h UT image, at the same wavelength (J band). The reddest colours are from the earlier image, the bluest from the later. The isophotes, linearly scaled every 10%, are from the 7:06 h UT J band image

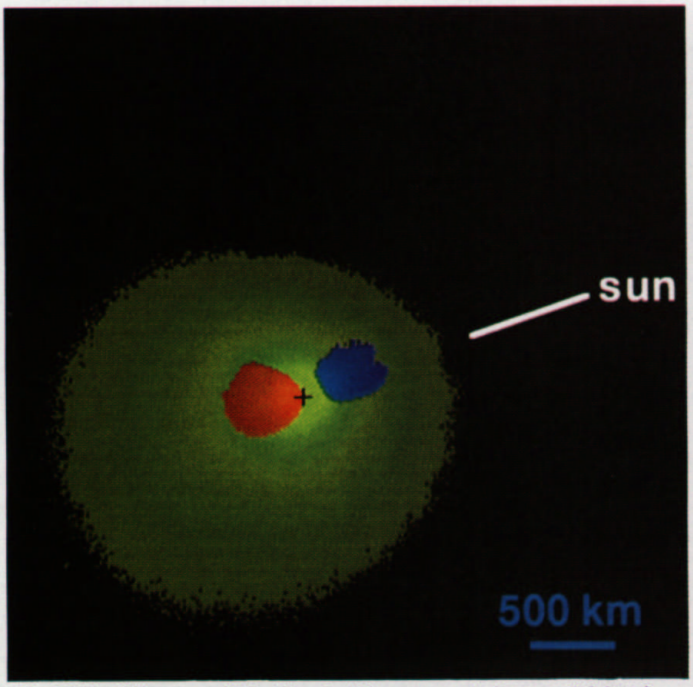

Fig. 3. [J–H] image of the Hyakutake comet, taken on 8 March, ~7:03 h UT. The colours indicate the dust colour: yellow for an index of 0.37 ± 0.05, blue for 0.30 ± 0.02, and red for 0.50 ± 0.03. The cross indicates the nucleus

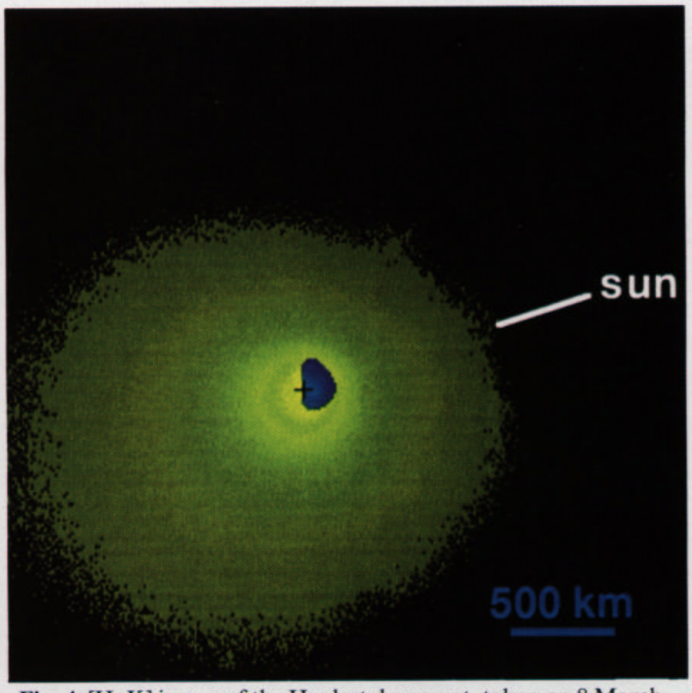

Fig. 4. [H–K] image of the Hyakutake comet, taken on 8 March, ~9:28 h UT: the comet as rotated of about 150° relatively to the [J–H] image. The colours indicate the dust colour: yellow for an index of 0.16 ± 0.05, and blue for 0.29 ± 0.05. The cross indicates the nucleus

theless, we do not detect any jet on the colour maps. This indicates that they have not a particular dust composition.

Conclusion

These observations of comet Hyakutake were the first attempt to image a coma in the near infrared with adaptive optics, achieving a sub–hundred kilometre spatial resolution. The images obtained demonstrate the feasibility of this technique and illustrate the interest of such observations. Another opportunity is offered with comet C/1995 O1 (Hale–Bopp), which will reach its perihelion 0.9 AU from the Sun on April 1997. A water-ice absorption band has already been detected in the infrared, as far as about 7 AU from the Sun (Davies *et al.*, 1995). Imaging this comet in the infrared as it approaches the Sun will offer a new opportunity to study the dust composition and distribution in the coma.

Acknowledgements. We thank the 3.6 m telescope ESO La Silla staff members, and in particular P. Bouchet and D. Le Mignant for their helpful assistance during the night of the observations. We are very grateful to J. Crovisier for his fruitful comments.

References

A'Hearn, M. F., Dwek, E. and Tokunaga, A. T. (1981) Where is the ice in comets? *Astrophys. J.* **248,** L147–151.

Beuzit, J. L. *et al.* (1994) *Proc. SPIE* 2201 , ed. M. A. Ealey and F. Merkle, pp. 955–961.

Campins, H. and Hanner, M. S. (1982) Interpreting the thermal properties of cometary dust. In *Comets*, ed. L. L. Wilkening, pp. 341–356. University of Arizona Press, Tucson, AZ.

Campins, H., Rieke, G. and Lebofsky, M. J. (1982) Infrared photometry of periodic comets Encke, Chernykh, Kearns-Kwee, Sphefan-Oterma, and Tuttle. *Icarus* **51,** 461–465.

Combes, M., Moroz, V. I., Crifo, J. F., Lamarre, J. M., Charra, J., Sanko, N. F., Soufflot, A., Bibring, J. P., Cazes, S., Coron, N., Crovisier, J., Emerich, C., Encrenaz, T., Gispert, R., Grigoyev, A. V., Guyot, G., Krasnopolsky, V. A., Nikolsky, Yu. V. and Rocard, F. (1986) Infrared sounding of comet Halley from Vega 1. *Nature* **321,** 266–268.

Davies, J, Geballe, T., Cruikshank, D., Owen, T. and De Burgh, C. Comet C/1995 01 (Hale–Bopp). *IAU Circular* **6225,** 1995.

Encrenaz, T., Engels, D. and Krautter, J. (1984) Near-infrared photometry of comet P/Crommelin. *A&A* **140,** L13–L15.

Hanner, M. S. (1981) On the detectability of icy grains in the comae of comets. *Icarus* **47,** 342–350.

Hanner, M. and Tokunaga, A. (1991) Infrared techniques for comet observations. In *Comets in the Post-Halley Era*, Vol. 1, pp. 67–91. Kluwer, Dordrecht.

IAU Circulars (1996) IAU Circulars, Nos. 6225, 6311, 6318, 6333, 6336, 6344, 6354, 6365.

Jorda, L., Schleicher, D., Millis, R., Lecacheux, J. and Colas, F. (1996) Comet C/1996 B2 (Hyakutake). *IAU Circular* **6344,** 1996.

Lecacheux, J., Jorda, L., Enzian, A., Klinger, J., Colas, F., Frappa, E. and Laques, P. (1996) Comet C/1996 B2 (Hyakutake). *IAU Circular* **6354,** 1996.

Lisse, C. M. and A'Hearn, M. F. (1996) Comet C/1996 B2 (Hyakutake). *IAU Circular* **6336,** 1996.

Maillard, J. P., Crovisier, J., Encrenaz, T. and Combes, M. (1987) The spectrum of comet P/Halley between 0.9 and 2.5 microns. *Astron. Astrophys.* **187,** 398–404.

Mason, C. G., Gehrz, R. D., Jones, T. J. and Williams, D. M. (1996) Comet C/1996 (Hyakutake). *IAU Circular* **6396,** 1996.

Ney, E. P. (1974) Infrared observations of comet Kohoutek near perihelion. *Astrophys. J.* **189,** L141–143.

Ney, E. P. (1974) Multiband photometry of comets Kohoutek, Bennett, Bradfield, and Encke. *Icarus* **23,** 551–560.

Saint-Pé, O., Combes, M. and Rigaut, F. (1993) Ceres surface properties by high-resolution imaging from Earth. *Icarus* **105,** 263.

Sagdeev, R. Z., Blamont, J., Galeev, A. A., Moroz, V. I., Shapiro, V. D., Shevchenko, V. I. and Szegö, K. (1986) Vega encounters with comet Halley. *Nature* **321,** 259–262.

Veeder, G. J. and Hanner, M. S. (1981) Infrared photometry of comets Bowell and P/Stephan-Oterma. *Icarus* **47,** 381–387.